DOI 10.1515/aot-2013-0052 — Adv. Opt. Techn. 2014; 3(1): 91–102

Research Article

Paul Johannes Jobst*, Olaf Stenzel, Mark Schürmann, Norbert Modsching, Sergiy Yulin, Steffen Wilbrandt, Dieter Gäbler, Norbert Kaiser and Andreas Tünnermann

Optical properties of unprotected and protected sputtered silver films: Surface morphology vs. UV/VIS reflectance

Abstract: The optical properties of opaque sputtered silver films are investigated and related to their surface morphology. As reference, an evaporated sample produced by thermal flash evaporation has been studied, too. Standard optical and electrical characterizations as well as scanning electron microscopy (SEM) and X-ray reflectometry have been carried out with unprotected silver films directly after deposition and reveal strong correlations between the corresponding characterization results. The aging behavior of the normal incidence reflectance has been studied over a time period of 36 weeks. Protected silver mirrors have been prepared by sputtering using silica and alumina as the protective coating. It is shown by model calculations that the main spectral features occurring in the reflectance spectra of as-deposited unprotected coatings, unprotected coatings after aging, and protected coatings can be reproduced assuming a rough silver surface covered by a corresponding ultrathin absorbing interface layer or overlayer.

Keywords: mixing model; protected mirror; reflectance spectra; silver; sputter deposition.

OCIS Code: 310.0310.

***Corresponding author: Paul Johannes Jobst,** Fraunhofer Institute for Applied Optics and Precision Engineering IOF, Albert-Einstein-Strasse 7, 07745 Jena, Germany; and Friedrich-Schiller-University Jena, Institute of Applied Physics, Abbe Center of Photonics, Albert-Einstein-Strasse 15, 07745 Jena, Germany, e-mail: paul-johannes.jobst@iof.fraunhofer.de

Olaf Stenzel, Mark Schürmann, Sergiy Yulin, Steffen Wilbrandt, Dieter Gäbler and Norbert Kaiser: Fraunhofer Institute for Applied Optics and Precision Engineering IOF, Albert-Einstein-Strasse 7, 07745 Jena, Germany

Norbert Modsching and Andreas Tünnermann: Fraunhofer Institute for Applied Optics and Precision Engineering IOF, Albert-Einstein-Strasse 7, 07745 Jena, Germany; and Friedrich-Schiller-University Jena, Institute of Applied Physics, Abbe Center of Photonics, Albert-Einstein-Strasse 15, 07745 Jena, Germany

1 Introduction and background

Mirror coatings are of crucial importance in many optical applications. They are essential parts of optical systems or devices where reflective surfaces are required. This study is focused on pure silver as the basic material. Opaque silver films have a higher reflectivity than aluminum in the visible spectrum of the light and gold up to the infrared spectral range [1–5]. Unfortunately, the silver reflectance is rather low in the ultraviolet range.

Today, silver has found application as an optical material in a much broader sense. Semitransparent silver films are incorporated into transmissive filter designs when broad blocking regions at longer wavelengths are specified. Moreover, nanostructured or silver island films are essential in applications that are utilizing plasmonic, hydrophobic, or antimicrobial effects [6–8]. The morphology of these films is discussed in numerous publications and was studied extensively [9–11]. If the silver island network starts to percolate and the film is grown to an opaque layer, the morphology and the silver film properties are completely different from the island films [12–14]. In particular, sputtered silver layers are reported to have highest VIS reflectance at a thickness of about 90 nm [15]. This allows their use as high-reflecting optical mirrors in very precise optical systems, e.g., in solar or astronomical applications [16–19].

Pure silver has a lower environmental stability than, e.g., aluminum as it has a strong affinity to corrosion but especially to sulfurous compounds [19–21]. For this reason, silver films usually need protection in optical systems with atmospheric contact. Indeed, protected and enhanced

silver mirrors are state of the art today, but nevertheless, every protecting layer starts growing on the blank silver surface, and the real structure of the latter will be of crucial importance for the ultimate performance of the protected mirror coating. Knowledge of the performance of the unprotected silver surface is also essential for optical *in situ* monitoring issues. Therefore, one focus of the present study is on the unprotected silver surface. The optimization of such systems starting with the silver reflectance supports the reliability and the efficiency of optical systems that are used for instance in optical measurement systems in modern astronomical applications. It is a notable fact that the evaporation technology provides better results with respect to maximum reflectance, but the sputtering technology is widely accepted and often chosen [17, 22–24] due to other reasons. Major issues are the better scalability of the sputtering process to almost any mirror size [25] and an excellent reproducibility over years. Another reason may be the better pinhole-free densification and better covering of the silver at the layer systems' edge thus leading to a more reliable protection effect [4].

Figure 1 shows the reflectance spectra of opaque silver films obtained basing on several literature studies. These studies were using different deposition technologies to deposit the silver films and different characterization methods to determine the optical constants [5, 26, 27].

Johnson and Christy used a fast and clean evaporation and exact characterization process. Their optical constants are likely to be closest to bulk silver values among the samples shown in Figure 1 as a smoothed version [28] of the data from [26]. Hass used an evaporation technique as well but deposited the films and determined the optical constants with a different method [27]. Here, the absolute reflectivity values were taken from [29] to plot the spectrum. Palik [5] uses a combination of literature values from [30–33], whose silver samples were evaporated or polished from polycrystalline silver.

The comparison of the spectra in Figure 1 shows significant differences in reflectance in some special regions of the spectra. This was already recognized by Palik [34], who found differences in optical constants of up to a factor of two as he compared the existing optical constants in the literature, which is further known under anomalies of optical constants [35]. Unfortunately, these studies do not discuss the reasons with respect to the material properties. Other studies that are dealing with the morphology of the deposited silver films via different deposition technologies do not discuss the interplay between morphology and optical properties of the film [36, 37].

In this paper, we basically investigate structure-related properties of optical silver films and connect the morphology and material properties of the deposited silver layers to their optical properties. Based on the results of surface characterization, a model is developed that may describe the optical properties of the measured films through specific properties of their surfaces. The crystalline structure of the deposited silver samples was characterized with X-ray diffraction analysis, and the surface roughness, mass density, and film thickness were determined by X-ray reflectometry. The silver electrical dc resistivity was determined with a four-point probe device, and top views of the silver film surfaces were taken with scanning electron microscopy (SEM).

2 Experimental details

2.1 Sample preparation

The silver films were deposited on B270 glass samples and crystalline Si-Wafers with <100> orientation. Before deposition, a detergent-supported ultrasonic cleaning line washed the samples in cleanroom conditions. Before deposition, the samples were pre-etched to remove residual water or other molecules that are still covering the substrates.

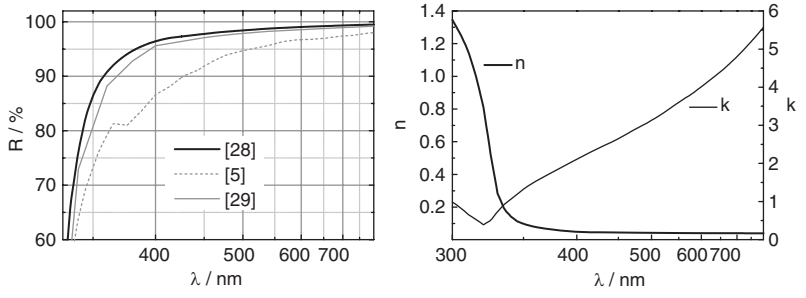

Figure 1 Left: reflectance spectra of opaque silver films as derived from literature data [5, 28, and 29]; right: optical constants of silver according to [28].

The conventional evaporation was performed in a Leybold Optics Syrus Pro 1100/F batch coater. The chamber was pumped via turbomolecular pump to a residual pressure of about 5×10^{-6} mbar, and silver with a purity of 4 N was flash evaporated via thermal evaporation out of a tungsten boat with a peak deposition rate of 6 nm/s. To prevent gaseous water in the chamber, a Meissner trap was installed. The deposition parameters for a typical evaporated sample (E1) are shown in Table 1.

The sputtered samples were prepared in an inline magnetron sputter system Systec SVS vacuum coatings Z750H. Equipped with a direct current power supply unit (dc magnetron sputtering), the process started, cryo-pumped at a residual gas pressure of about 2×10^{-6} mbar. The silver target had a purity of 4 N on a target area of 75×10 cm^2. The sputtering gas species was argon. The process parameters were varied in three ways resulting finally in 18 samples. The deposition parameters for the three most significant samples (S1–S3) are listed in Table 1.

With respect to the power density, the deposition rate of four representative samples varied according to Table 1, whereas the working pressure varied from low to high. The substrate temperature was varied between room temperature to a maximum of about 77°C.

In a subsequent step, sputtered silver mirrors protected with either silica or alumina layers have been prepared for comparison purposes. Main design parameters are summarized in Table 2.

Table 1 Key deposition parameters of four representative unprotected silver samples.

Sample code	S1	S2	S3	E1
Deposition rate (nm/s)	0.5	1.9	0,07	3
Working pressure (mbar)	2×10^{-3}	2×10^{-3}	1.2×10^{-2}	5×10^{-6}
Deposition temperature (°C)	20	77	77	36

Table 2 Main construction parameters of the protected silver mirrors.

Sample code	Type of silver surface	Protection material	Thickness of the protection layer (nm)
S2+SiO_2 thick	S2	SiO_2	169
S2+SiO_2 thin	S2	SiO_2	113
S2+Al_2O_3	S2	Al_2O_3	107
S3+Al_2O_3	S3	Al_2O_3	109

2.2 Sample characterization

In order to visualize the surface of the deposited silver films in a direct manner, an SEM device of Zeiss Sigma FE was used. To detect a possible content of noble gas in the layers, energy-dispersive X-ray spectroscopy (EDX) has been carried out using the same SEM with an applied silicon drift detector (Oxford Instruments GmbH Inca X-act).

A Bruker AXS D8 advance was used for X-ray reflectometry in grazing incidence geometry with a CuKα source (radiation wavelength of 0.154 nm) to identify the surface roughness σ_{rms} [root mean square (rms)], material density ρ, and the thickness d of the layers. The measurement uncertainties for these three units are $\Delta d/d=0.3\%$, $\Delta\rho/\rho=3\%$, and $\Delta\sigma_{rms}/\sigma_{rms}=10\%$.

A Bruker AXS D 5005 was used for X-ray diffraction in a Bragg-Brentano geometry (θ-2θ geometry) with a CuKα source (radiation wavelength of 0.154 nm). The peaks in the diffractogram that are indicating crystallite structures in the deposited film were evaluated with the Scherrer equation to calculate the grain sizes D in the direction of the silver film growth [38].

$$D=\frac{K\cdot\lambda}{FWHM(2\theta)\cdot\cos\theta}$$

K is the Scherrer form factor, and it is 0.94 for cubic crystal lattices. λ is the radiation wavelength. FWHM(2θ) is the full width at half of the maximum at the peak of the central detection angle in radian.

The resistivity measurement was done with a device based on the four-point method. The reflectance R of the sample was measured with a PerkinElmer Lambda 950 spectrophotometer in the UV-VIS-NIR spectral range. Measurements have been carried out for 6°, 45°, and 60° angles of incidence using VN accessories for absolute measurements [39]. Systematic measurement errors in reflectance do not exceed 0.5% and have no impact on the ranking of the samples with respect to their reflectance.

Aging effects have been investigated by repeated reflectance measurement over a longer span. We emphasize here that the main focus of this study is directed toward sputtered silver layers. The evaporated sample has been deposited for reference purposes only at a later time. Therefore, the aging effects are expected to be more pronounced in the sputtered samples.

3 Characterization results

Figure 2 displays the measured reflectance spectra in the visible range of four representative silver samples (see Table 1) compared to literature values. These spectra have

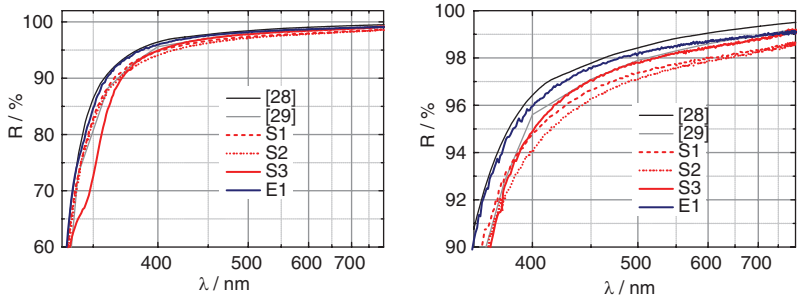

Figure 2 Measured reflectance R spectra of the four representative deposited samples compared with literature values; left: overview; right: region of high reflectance.

been recorded within 24 h after layer deposition. The diagram thus highlights the impact of different sputtering parameters on the optical performance. However, the evaporated sample E1 remains superior with respect to its reflectance, which is close to the reflectance spectrum simulated basing on the optical constants of Johnson and Christy.

Table 3 gives an overview about the most important measured values. The thicknesses of the deposited silver layers are between 110 nm up to 150 nm and indicate opaque silver layers. The roughness was measured twice: after deposition and after 1 year again. The grain sizes of the silver layers where extracted according to Scherrer's equation [38] using reflection from the (111) and (200) planes of the cubic silver parallel to the silver surface (corresponding to patent 04-0783 in JCPDS [40]). Each resulting pair of values was averaged and is listed in Table 3.

Figure 3 shows a SEM top view of the four presented samples. The sputtered films exhibit a granular texture with different feature sizes. For the evaporated film, the basic granular features have the same shape as those of the sputtered films, but they are interrupted by very large, flat silver slabs with an own texture on them at the visible film surface at least.

Table 3 Primary measurement results obtained from unprotected samples.

Sample code	S1	S2	S3	E1
XRR – thickness (nm)	144.9	137.8	110.1	148.8
R at 440 nm after deposition (%)	96.4	96.0	96.8	97.4
DC resistivity (10^{-8} Ωm)	2.7	3.5	2.3	1.9
XRR – roughness after deposition (nm)	1.7	1.5	2.9	2.3
XRR – roughness after 1 year (nm)	2.1	1.7	3.8	–
XRR – mass density after 1 year (g/cm^3)	10.5	10.4	10.2	–
XRD – mean grain size (nm)	19.5	16.6	20.9	25.5

The images give an idea of the grain size and the surface texture differences of the films according to their deposition properties. An additional EDX spectroscopy measurement did not show any impurities or embedded particles like argon in the silver films within its detection limits.

Once these silver coatings are not protected, their surfaces are subject to degradation as a result of aging in atmospheric conditions. This surface degradation will surely have an effect on their reflectance. In order to give an impression on the magnitude of the effect, in Figure 4 (left), the drop in normal incidence reflectance with time is visualized for λ=440 nm.

On the right in Figure 4, UV/VIS reflectance spectra of sample S3 as recorded at different levels of aging are demonstrated. It is obvious that, already for the fresh sample, a feature appears in the reflectance spectrum around 340 nm, which does not originate from a smooth silver surface when assuming the optical constants from Figure 1 [28]. We assign this spectral feature to the excitation of localized plasmon modes at the rough silver surface (Figure 3) [41]. The obvious effect of aging is in a slight red shift of this feature, accompanied with the appearance of a spectrally broad absorption tail, which extends deeply into the VIS. In the appendix, we will present a model, which reproduces this kind of spectrum in terms of the mentioned rough silver surface, covered with a silver sulfide-containing debris layer, which is formed as the result of the aging process.

4 Modeling approach

4.1 Model geometry

Based on the findings from the previous section, as well as the study of Bennett et al. [42], the surface of the silver

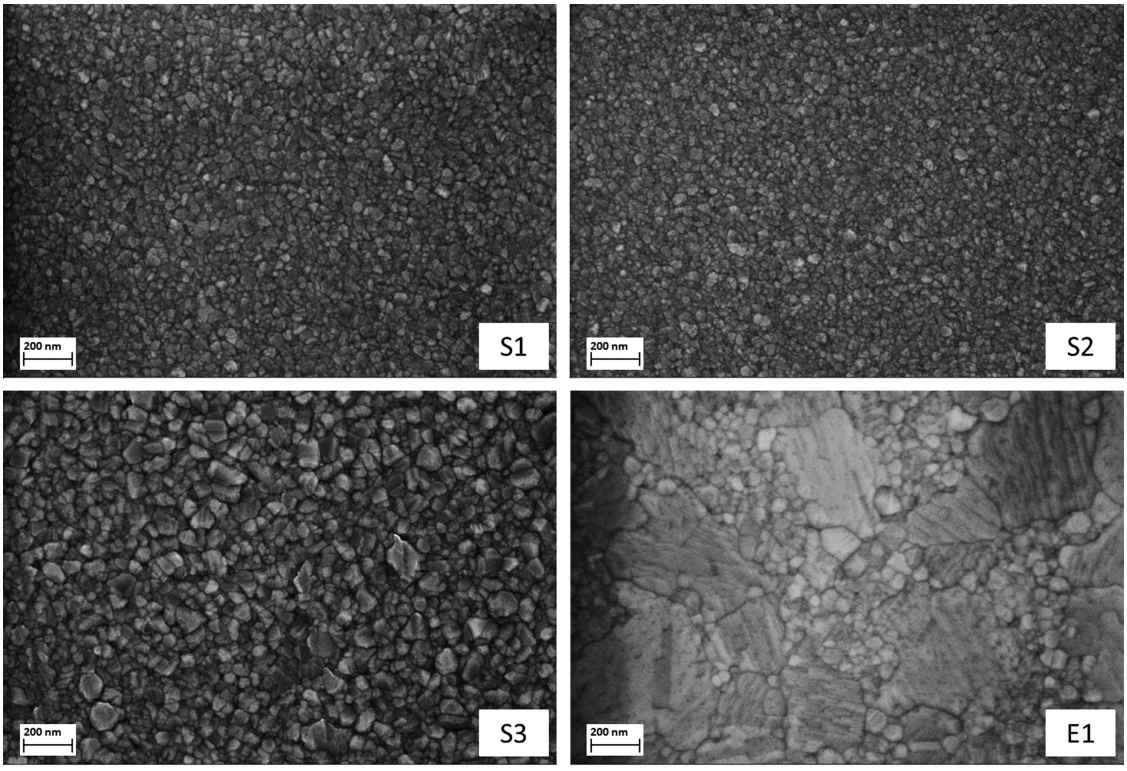

Figure 3 SEM images of the surface morphology of the four representative samples (after deposition).

mirrors has been modeled in terms of a mixing model approach. Details of this calculation are given in the appendix; we focus, here, only on the main model assumptions and the major results. Thus, the assumed structure of the model surface is given in Figure 5. In agreement with Figure 3, the essential model feature is the assumption of a rough interface between the top of the silver film and the adjacent medium. The distinction between fresh unprotected silver, unprotected silver after aging, and protected silver is in the choice of the optical properties of the adjacent medium.

4.2 Application of the model to aging effects

According to Figure 5 (left), aging effects are taken into account assuming that the rough silver surface is overcoated by a rather thin tarnish or debris layer formed as a result of chemical degradation. That debris layer is supposed to be composed from silver, silver sulfide, and air. As explained in the Appendix, these assumptions allow simulating the measured reflectance of aged silver films. Figure 6 shows the result of fitting the reflectance spectra (normal and AOI of 60°) for the

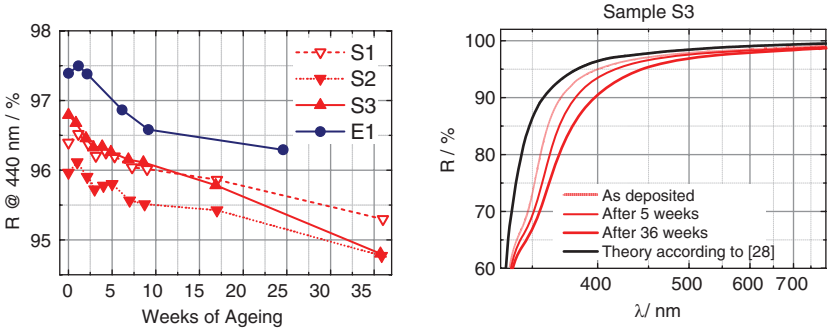

Figure 4 Left: decrease in normal incidence reflectance at λ=440 nm of unprotected silver layers with time; right: section of normal incidence spectra of sample S3 as the result of aging.

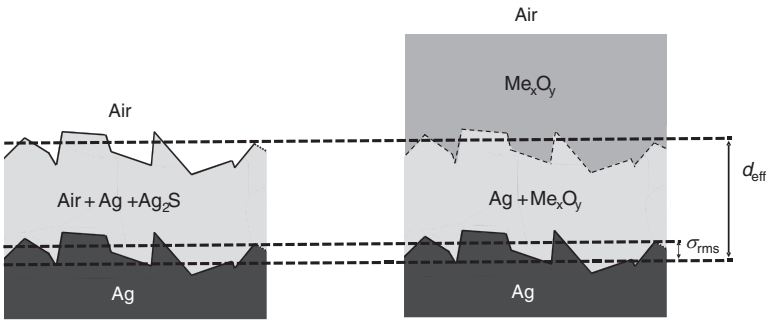

Figure 5 Assumed surface geometry. Left: model geometry for describing aging effects in unprotected silver surfaces; right: model geometry for the case of a silver surface protected (and enhanced) by a metal oxide coating.

samples S1, S2, S3, and E1 after aging at atmosphere for 36 weeks.

We see that the model is able to reproduce the major features of the spectra. Best modeling results are clearly observed for the samples with smallest grain size. This is not astonishing because the underlying mixing models are formulated within the quasistatic approximation, which requires the characteristic dimension of any inhomogeneity to be much smaller than the wavelength. This assumption might be violated in the case of samples S3 and E1. We mention that remaining discrepancies between experiment and theory are most pronounced for the p-polarization spectra (see Appendix). Much better fits are achieved for the 6° AOI case, which is tackled in the simulation as normal incidence.

4.3 Application of the model to protected silver surfaces

In application to protected layers, we make use of the geometry shown in Figure 5 on the right. Instead of a debris layer, we are now considering an interface region where a certain amount of silver is embedded into the oxide layer material, i.e., a mixture layer. Concerning the effective thickness of this mixture layer as well as filling factor and particle shapes, we use exactly the same parameters, which have been established for simulating the aging effects. Thus, no further fitting has been performed. On top of the mixture layer, the protected mirror design is completed by the pure oxide layer. This way, we come to the simulated spectra shown in Figure 7 together

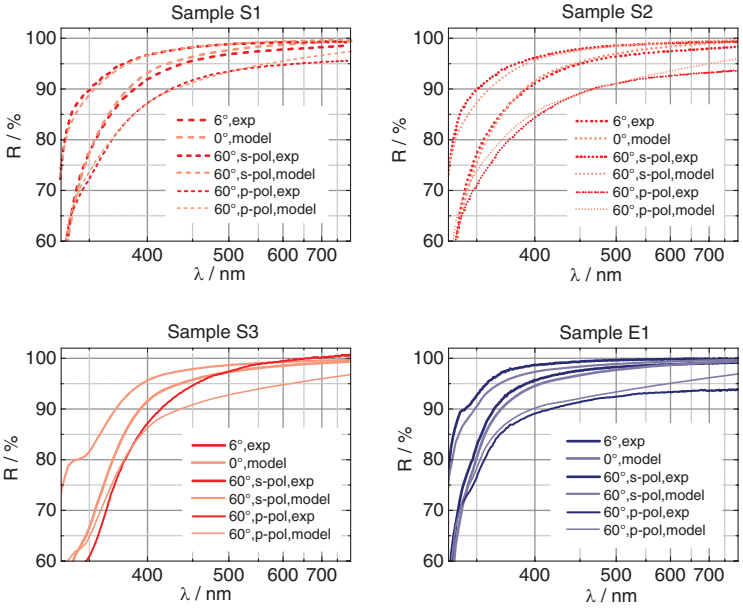

Figure 6 Comparison between experimental reflectance spectra and the results of spectra modeling. 'exp' denotes measured spectra after 36 weeks of aging and 'model' the result of the simulation according to the appendix.

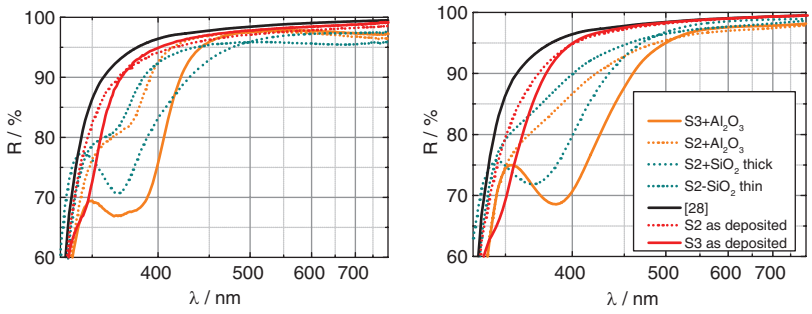

Figure 7 Comparison of reflectance spectra of fresh unprotected and protected silver mirrors. Left: experimental spectra at an AOI 6°; right: simulation for assumed normal incidence.

with the measured spectra of the corresponding samples. The simulation of the fresh unprotected silver surface has again been performed in terms of the model in Figure 5 on the right, while virtually replacing the oxide fraction by air in the calculations.

Applying the interface model established for the bare silver films to the protected silver films and only exchanging air and Ag_2S for Al_2O_3 or SiO_2, we found already a very good agreement between simulation and experimental data (Figure 7) without any fitting of the model parameters. However, we cannot exclude the existence of silver oxide at the interface. According to [43], the optical constants of AgO and Ag_2O are not sufficiently different from the optical constants of Al_2O_3 and SiO_2 to exclude the existence of a very thin (a few nanometers) silver oxide film at the interface by means of optical spectroscopy. Adding a very thin silver oxide film to the model and fitting its thickness together with the other model parameters for the protected silver films might further improve the agreement between simulated and experimental spectra. However, the number of fitting parameters will be increased this way, so that model becomes much more complex, and the fitting results might be less meaningful. Regarding the very good agreement of the simulations based on the proposed very simple model, we chose not to include a potential silver oxide layer or other potential interface layers.

5 Discussion and conclusions

The main topic of this paper is clearly the discussion of the relationship between morphological properties of the films and their optical performance. Nevertheless, our data also allows for establishing basic correlations between deposition parameters and the film structure, and we will start the discussion with this subtopic.

First of all, we found that an increase in sputtering power (which is accompanied by an increase in deposition rate) results in films with smaller grain sizes. If the substrate temperature during deposition is elevated, the grain sizes tend to increase as well, which reveals a trend opposite to an increase in deposition power. A comparison of the grain sizes from Figure 3 and the mean grain sizes from Table 3 that were extracted from the crystallite feature measurement via XRD confirms that larger measured grain size dimensions are accompanied by larger grains in the SEM image. A further possibility to influence the particle energy during sputtering is to adjust the residual gas pressure in the deposition chamber. In combination with the decreased sputtering power, we could produce sputtered silver films with rather large grain sizes, while the mean grain size is still smaller than for the evaporated sample E1.

From Section 2.2, it is also evident, that larger grain sizes at the silver surface are accompanied by a higher VIS reflectance. Thus, it can be concluded that the grain size is one main driver for the high reflectance of the evaporated sample. Optimization of the sputtering process should therefore pursue the formation of large grains. Based on the EDX measurement results, we have no hint on a relevant impact of impurities on the reflectance of the sputtered samples.

It thus turns out that the grain size is crucial, and grain boundaries are expected to have an important impact on the optical properties. They are influencing the electrical conductivity of the layer and are, therefore, according to Drude's theory, directly responsible for the optical behavior of the film in vacuum or immediately after deposition. This is in agreement with the data from Table 3. The resistivity values are in inverse ratio to the reflectivity values at 440 nm, and this correlation is highlighted in Figure 8. The 'bulk-like silver' value is a combination of the reflectance value derived from the optical constants of Johnson and Christy [26] and the bulk silver resistivity value [44]. The other extra value (theoretical maximum) corresponds to an ideal metal with infinite conductivity and 100%

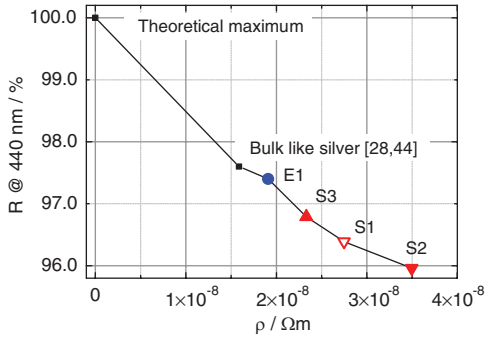

Figure 8 Correlation of dc resistivity and reflectance of silver films.

reflectance. The measured data are in reasonable accordance to these special points.

Thus, larger grains induce a lower resistivity and therewith a higher reflectance. The flat large grains of the sample E1 support the reflectance of the evaporated sample in particular.

Unfortunately, the grain size cannot be magnified at will. With increasing grain sizes, the surface gets rougher. However, this is not as crucial as the grain dimensions are. The roughness values (Table 3) are much lower than the wavelength, so that no crucial changes in reflectance are expected when the roughness varies in the range of 1 or 2 nm. On the other hand, the Fermi velocity of electrons in silver is 1.4×10^6 m/s [45]. Combined with characteristic conduction electron relaxation times in bulk silver of 16–37 fs [46, 47], this leads to characteristic propagation paths in the region between 22 and 52 nm. This is exactly the range of grain dimensions in our samples and explains the impact of the lateral grain size on the optical properties of as-deposited layers.

After aging, the situation becomes more complicated. The particular shape of the surface profile is expected to have an impact on the properties of what we called a debris layer in Section 4. In any case, a clean silver surface reacts with sulfurous compounds if they are present. Therefore, aging results in the formation of an overlayer, which has an impact on the reflectance. In terms of the proposed model, the normal incidence reflectance of all aged layers could be well reproduced, and so the main features of oblique incidence spectra could be reproduced sufficiently as well. All in all, the experimental results from Figures 2–4 and Figures 7 and 8, combined with the results of the model calculation, reveal the following picture:

I. Depending on the deposition type and conditions, as-deposited silver layers show a characteristic surface morphology (Figure 3), which gives rise to differences in their reflectance. The electrical conductivity of the coatings is in direct correlation with the VIS reflectance. Moreover, the roughness leads to the formation of a more or less pronounced absorption feature in the UV reflectance spectrum, which is located around 340 nm.
II. When exposed to air, chemical degradation leads to the formation of an absorbing debris layer on the rough silver surface. In terms of the model introduced in the Appendix, the combined action of the interface roughness and the absorbing debris layer results in a spectral shift of the plasmonic absorption feature, combined with the appearance of a spectrally broad absorption tail mainly originating from the intrinsic absorption of silver sulfide [42]. This mechanism thus explains the observed loss in reflectance over the entire UV-VIS spectral region as a result of aging.
III. When layers are protected by a dielectric protection film, the rough silver surface does still give rise to certain plasmonic absorption. This is a fact that we will have to accept. But depending on the choice of the protection material, the plasmonic feature shifts to wavelength values somewhat different to what has been shown in Figure 4 (right). This allows some additional flexibility in tailoring the UV performance of the mirror. Moreover, with a dielectric cover layer, spectrally selective enhancement effects caused by constructive interference effects become accessible [18].
IV. Because of its impact on both reflectance and electrical conductivity, the silver film surface quality might be controlled during deposition by *in situ* measurements of the reflectance and electrical conductivity of the growing film. Depending on the results of such an *in situ* characterization, the properties (material, thickness) of the dielectric protection layer might be adapted on-line to the specific quality of the metal film being produced, in order to optimize the properties of the final protected mirror. Newly developed *in situ* reflectance monitors have an accuracy in reflectance measurement of around 0.5% [48], which clearly allows distinguishing between silver films like those shown in Figure 8.

Acknowledgment: The authors appreciate the assistance of Sabrina Wolleb and Stefan Schwinde for the preparation and analysis of the samples in terms of the SEM investigations and Nancy Kaufmann for continuously measuring the optical properties of the samples in reflectance. Regarding the four-point probe measurement performed by Astrid Bingel and relating to help in consistent preparation of the figures by Josephine Wolf, the authors are very grateful, too.

Received September 6, 2013; accepted October 21, 2013; previously published online November 23, 2013

Appendix

A model for calculating the effective optical constants of an absorbing overlayer, applied to the optical properties of the rough silver surface

A1. Application to aging effects of unprotected silver

As is evident from Figure 2, all of the measured reflectance spectra tend to reveal lower reflectance values as it would follow from the calculation at the air/silver interface with theoretical optical constants taken from the source [28]. This is already an indication that the real silver films cannot be described assuming an ideal air-silver interface with optical constants taken from standard reference sources. Instead, one will have to either correct the optical constants of the silver fraction or, alternatively, to consider a more complicated surface geometry, for example, in terms of a thin surface overlayer.

It is easy to verify that the second approach must be favored. Indeed, at any single smooth and plane interface, Abeles condition [49] must be fulfilled, so that at 45° incidence, $R_s^2=R_p$ must hold no matter which particular optical constants are assumed. However, a glance at Table A1 confirms that for our samples, $R_s^2>R_p$ is generally fulfilled.

Hence, the single interface approach is inconsistent anyway, and the optical surface properties need to be modeled assuming a somewhat more complicated surface morphology. Moreover, the fact that the p-polarized reflectance is lower than expected indicates the presence of an ultrathin absorbing overlayer on the metal surface. This indication is consistent with the findings from Figure 3. Here, a relevant surface pattern is evident in all of the samples, which likely gives rise to light absorption. Moreover, the dominant lateral surface harmonics correspond to spatial dimensions still lower than the wavelength of the light relevant in this study. Therefore, according to [50], the surface pattern gives rise to a small-scale roughness, which does not cause any relevant scatter losses, and can be modeled by a fictive thin and optically homogeneous overlayer. The principal idea is therefore to develop a two-layer model, where a rather 'ideal' thick opaque silver film is covered by an ultrathin absorbing overlayer. We note that the mentioned assumption is best fulfilled for samples S1 and S2, while samples S3 and E1 tend to show rather large, flat grains. This could give rise to particular difficulties when fitting their p-polarized reflectance because of possible violations of the quasistatic approximation [51] combined with a relevant anisotropy of the grain shape.

Table A1 Reflectance data after aging of 36 weeks.

$R_{45°}$ at 440 nm/%	S1	S2	S3	E1
R_s	97.4	96.0	96.1	98.4
R_s^2	94.9	92.2	92.4	96.8
R_p	92.4	91.8	91.7	95.4
R_s^2-R_p	2.5	0.4	0.7	1.4

Concerning the thickness and optical properties of that overlayer, an additional difficulty has to be considered. As is seen from Figure 4, aging of the films at atmosphere leads to a permanent decrease in reflectance, thus, indicating that the effective thickness and optical properties of the overlayer must change with time [42]. This is the result of the formation of a silver sulfide tarnish layer, which is, in turn, the result of a chemical degradation process and concerns all samples in a similar manner. Thus, the reflectance decrease dR/dt with time t is, on average, similar for all layers (Figure 4, left). On the other hand, differences in deposition method and conditions seem to have major impact on the reflectance R(t=0) of the as-deposited samples, most probably through differences in the surface morphology. A realistic modeling of the optical properties of unprotected silver films should, therefore, include both the effects of surface morphology and chemical degradation. In the following, we will present a simple model that takes into account both of these mechanisms. The goal is to demonstrate that a qualitative reproduction of the optical properties of all samples is possible when assuming a simple film model, where a bulk silver fraction with a rough surface is covered by a thin debris (or tarnish) fraction, which can be represented as a mixture of silver, silver sulfide [42], and air.

The geometrical aspects of the assumed model have been presented in Figure 5 on the left.

Basically, the layer model considers a rough silver surface, as evident in Figure 5, covered with a rather flimsy debris fraction, which may contain fractions of silver, silver sulfide, and air. The challenge was to reproduce main spectral features of the normal incidence reflectance

spectra as well as those recorded at an AOI of 60° (s- and p-polarization).

We mention at the very beginning, that the introduction of a pure sulfide debris layer did not lead to a satisfying reproduction of the measured spectra. This was particularly evident in the case of p-polarization. We, therefore, made use of typical mixing model approaches [51].

In the first step, a mixture of silver and silver sulfide has been modeled in terms of Bruggemans mixing model assuming corresponding filling factors of 50% and a depolarization factor of L=1/3. With these advance, we tried to model the result of the chemical degradation mechanism. This approach led us to the calculation of effective dielectric function of the solid fraction ε_{sf} of the debris layer. It is related to the dielectric functions of silver ε_{Ag} and silver sulfide ε_{Ag2S} via:

$$0=\frac{\varepsilon_{Ag}-\varepsilon_{sf}}{\varepsilon_{Ag}+2\varepsilon_{sf}}+\frac{\varepsilon_{Ag_2S}-\varepsilon_{sf}}{\varepsilon_{Ag_2S}+2\varepsilon_{sf}} \tag{A1}$$

In a second step, the full debris layer is assumed as a system of solid slices described in terms of the above-calculated dielectric function, embedded in air. Therefore, for the calculation of the full dielectric function of the debris layer, the Maxwell Garnett model has found application [52]. Best results have been obtained assuming a rather small volume filling factor of the solid fraction of 5%. It is, therefore, modeled as a rather flimsy surface cover. In order to comply with the statistical character of the pancake geometry of the surface slices seen in Figure 3, the lateral depolarization factor L of the inclusions was modeled through a rather broad statistical distribution g(L) centered at approximately L=0.5. For the effective dielectric function of the debris layer ε_{dl}, we thus have (compare [52]):

$$\varepsilon_{dl}=\int_0^1 g(L)\cdot\frac{1+\dfrac{0.05(1-L)(\varepsilon_{sf}-1)}{1+(\varepsilon_{sf}-1)L}}{1-\dfrac{0.05L(\varepsilon_{sf}-1)}{1+(\varepsilon_{sf}-1)L}}dL \tag{A2}$$

The concrete shape of the assumed normalized distribution g(L) was simulated assuming an assembly of ellipsoids with stochastically distributed main axes ([52]) and is shown in Figure A1.

Finally, in the third step, the full surface overlayer with effective dielectric function ε_{eff} and geometrical thickness d_{eff} has been assumed as a mixture of Ag spikes embedded into the previously calculated debris fraction (Figure 5). This way, the properties of the surface morphology are explicitly considered through filling factor p_{Ag} and

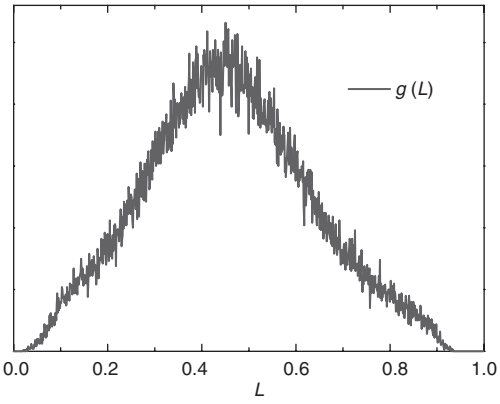

Figure A1 Assumed normalized depolarization factor distribution in Eq. (A2).

the depolarization factor distribution of the silver spikes. The latter as well as the thickness of the overlayer have been used as fitting parameters to comply with the specifics of the particular sample in terms of the approach:

$$\varepsilon_{eff}=\varepsilon_{dl}\int_0^1 g_{Gauss}(L)\cdot\frac{1+\dfrac{p_{Ag}(1-L)(\varepsilon_{Ag}-\varepsilon_{dl})}{\varepsilon_{dl}+(\varepsilon_{Ag}-\varepsilon_{dl})L}}{1-\dfrac{p_{Ag}L(\varepsilon_{Ag}-\varepsilon_{dl})}{\varepsilon_{dl}+(\varepsilon_{Ag}-\varepsilon_{dl})L}}dL \tag{A3}$$

In this third step, a normal distribution $g_{Gauss}(L)$ has been postulated, while the mean depolarization factor <L> and its standard deviation δL are tackled as fitting parameters. Throughout the full simulation, the optical constants of silver have been taken from [26], and those of the sulfide from [42]. The effective optical constants of the overlayer are finally obtained from the relation:

$$n_{eff}+ik_{eff}=\sqrt{\varepsilon_{eff}} \tag{A4}$$

The resulting effective optical constants of the overlayer are visualized in Figure A2; the main fitting parameters are given in Table A2. It was possible to perform the fits leaving the mean depolarization factor fixed. Only the effective thickness of the debris layer, the silver filling factor, and the standard deviation δL have been varied in order to account for the specifics of the different samples.

The used optical constants of silver sulfide were based on [42] and are shown in Figure A2 on the left. The corresponding effective optical constants of the four simulated overlayers are finally shown in Figure A2 on the right. Note the plasmonic absorption peak around 350 nm – it arises from the simulation step according to Eq. (A3) and appears connected to the surface texture of the coatings. In the reflectance spectrum, it gives rise to the dips in reflectance

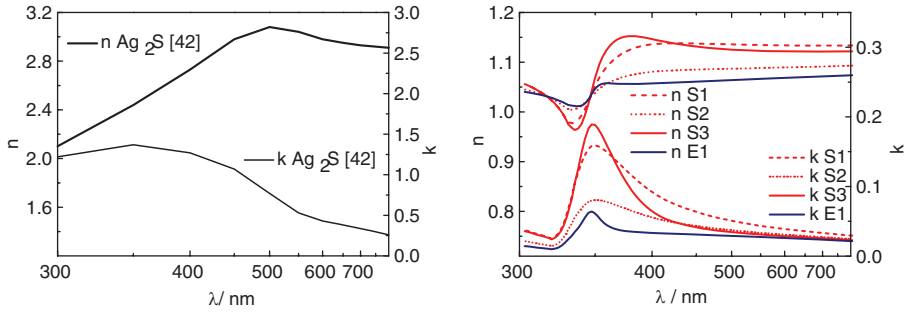

Figure A2 Left: optical constants of Ag_2S that were used based on [42]; right: modeled effective optical constants of the surface overlayer.

Table A2 Overview of fitting parameters.

Sample code	Effective thickness d_{eff} of the overlayer (nm)	p_{Ag} (%)	<L>	δL
S1	10	3.8	0.42	0.15
S2	20	1.5	0.42	0.15
S3	17	3.6	0.42	0.1
E1	15	0.5	0.42	0.04

around 350 nm, which appear more or less pronounced in the experimental UV reflectance spectra (Figure 6). The broad absorption tail in the VIS originates instead from the mixture of silver and silver sulfide as introduced in Eq. (A1), i.e., as a result of the chemical degradation process.

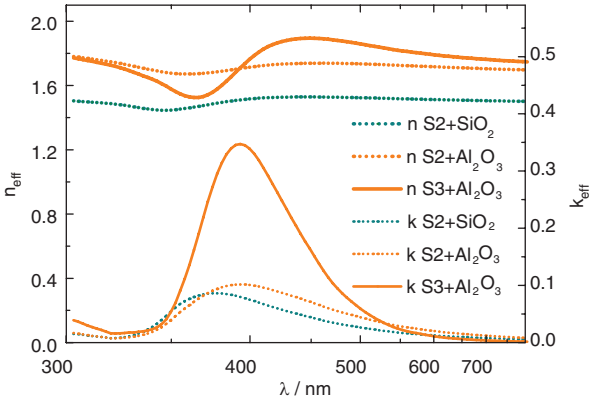

Figure A3 Modeled effective optical constants for the interface layers between silver and an oxide coating.

A2. Application to protected silver mirrors

In Figure 5 (right), the modification of the model to protected silver mirrors is visualized. There is no necessity to model a debris fraction in terms of Eqs. (A1) and (A2); instead, Eq. (A3) has been applied to model the overlayer immediately, replacing the dielectric function of the debris layer by that of the oxide material. Effective optical constants of the interface layer have again been calculated by means of Eq. (A4), while the corresponding construction parameters have been assumed completely identical to those introduced in Table A2. Thus, no more fitting was accomplished, but the spectra shown in Figure 7 (right) are the result of a primitive forward search procedure. The corresponding effective optical constants of the interface layers are visualized in Figure A3. The plasmon absorption peaks are still present, but shifted to longer wavelengths when comparing with Figure A2. According to theoretical considerations outlined in [41], these absorption features will even occur in the reflectance spectra of fully percolated and opaque silver layers, as long as the surface appears corrugated.

References

[1] A. Macleod, P. Soc. Photo-Opt. Ins. 8168, 816802 (2011).
[2] W. G. Driscoll and W. Vaughan, in 'Handbook of Optics', Ed. By W. G. Driscoll (McGraw-Hill, New York, 1978) pp. 8–92.
[3] D. E. Gray, in 'American Institute of Physics Handbook', Ed. By D. E. Gray (McGraw-Hill, New York, 1972) pp. 6–157.
[4] M. R. Jacobson, R. C. Kneale, F. C. Gillett, K. Raybould, J. F. Filhaber et al., P. Soc. Photo-Opt. Ins. 3352, 477 (1998).
[5] E. D. Palik, in 'Handbook of Optical Constants of Solids', Ed. By E. D. Palik (Academic Press, San Diego, 1998) pp. 280–387.
[6] S. Pillai, K. R. Catchpole, T. Trupke and M. A. Green, Jpn. J. Appl. Phys. 101, 093105 (2007).
[7] S. T. Dubasa, P. Kumlangdudsanab and P. Potiyarajb, Colloids Surf. A 289, 105–109 (2006).
[8] L. Shen, J. Ji and J. Shen, Langmuir 24, 9962–9965 (2008).

[9] S. Yoshida, T. Yamaguchi and A. Kinbara, J. Opt. Soc. Am. 61, 463–469 (1971).
[10] T. C. Huang, G. Lim, F. Parmigiani and E. Kay, J. Vac. Sci. Technol. A 3, 2161–2166 (1985).
[11] M. Marinov, Thin Solid Films 46, 267–274 (1977).
[12] C. Charton and M. Fahland, Surf. Coat. Technol. 142–144, 175–180 (2001).
[13] R. Dannenberg, E. Stach, J. R. Groza and B. J. Dresser, Thin Solid Films 379, 133–138 (2000).
[14] J. Greiser, P. Müllner and E. Arzt, Acta Mater. 49, 1041–1050 (2001).
[15] M. Vergöhl, N. Malkomes, B. Szyszka, F. Neumann, T. Matthée et al., J. Vac. Sci. Technol. A 18, 1632–1637 (2000).
[16] D. -Y. Song, R. W. Sprague, H. A. Macleod and M. R. Jacobson, Appl. Optics 24, 1164–1170 (1985).
[17] N. L. Thomas, J. D. Wolfe, J. C. Farmer, P. Soc. Photo-Opt. Ins. 3352, 580–586 (1998).
[18] M. Schürmann, P. J. Jobst, S. Yulin, T. Feigl, H. Heiße et al., P. Soc. Photo-Opt. Ins. 8450, 84502K (2012).
[19] A. Feller, N. Krishnappa, O. Pleier, J. Hirzberger, P. J. Jobst et al., P. Soc. Photo-Opt. Ins. 8450, 84503U (2012).
[20] T. E. Graedel, J. Electrochem. Soc. 139, 1963–1970 (1992).
[21] D. K. Burge, H. E. Bennett and E. J. Ashley, Appl. Opt. 12, 42–47 (1973).
[22] M. Boccas, T. Vucina, C. Araya, E. Vera and C. Ahhee, Thin Solid Films 502, 275–280 (2006).
[23] M. Schneermann and M. Groessl, Messenger 88, 4–5 (1997)
[24] R. R. Pillai, K. K. Sanjth, K. Mohanachandran, N. Sakhamuri, V. Shukla et al., P. Soc. Photo-Opt. Ins. 8444, 844428 (2012).
[25] J. D. Wolfe, D. M. Sanders, S. Bryan and N. L. Thomas, P. Soc. Photo-Opt. Ins. 4842, 343–351 (2003).
[26] P. B. Johnson and R. W. Christy, Phys. Rev. B 6, 4370–4379 (1972).
[27] G. Hass, in 'Applied Optics and Optical Engineering', Ed. By R. Kingslake (Academic Press, New York, 1965) p. 309.
[28] Optical constants from in-house database, in this case essentially a smoothed version of the data from [26].
[29] R. Wilson, in 'Reflecting Telescope Optics', Ed. By R. Wilson (Springer-Verlag, Berlin, 2001) pp. 423–429.
[30] H. -J. Hagemann, W. Gudat and C. Kunz, J. Opt. Soc. Am. 64, 742–744 (1975).
[31] G. Leveque, C. G. Olson and W. Lynch, Phys. Rev. B 27, 4654–4660 (1983).
[32] P. Winsemius, F. F. van Kampen, H. P. Lengkeek and C. G. van Went, J. Phys. F Met. Phys. 6, 1583–1606 (1976).
[33] B. Dold and R. Mecke, Optik 22, 435–446 (1965).
[34] E. D. Palik, in 'Handbook of Optical Constants of Solids III', Ed. By E. D. Palik (Academic Press, San Diego, 1998) pp. 6–8.
[35] C. V. Fragstein and H. Römer, Zeitschrift für Physik 151(1), 54–71 (1958).
[36] N. Maréchal, E. Quesnel and Y. Pauleau, Thin Solid Films 241, 34–38 (1994).
[37] K.-F. Chiu, M. G. Blamire and Z. H. Barber, J. Vac. Sci. Technol. A 17, 2891–2895 (1999).
[38] P. Scherrer, Göttinger Nachrichten 2, 98–100 (1918).
[39] O. Stenzel, S. Wilbrandt, K. Friedrich and N. Kaiser, Vak. Forsch. Prax. 21, 15–23 (2009).
[40] Joint Committee for Powder Diffraction Standards, Powder Diffraction File, International Center for Diffraction Data, Swathmore, PA, Card 4-784 (1988).
[41] H. Raether, in 'Surface Plasmons on Smooth and Rough Surfaces and on Gratings', Ed. By G. Höhler and E. A. Niekisch (Springer-Verlag, Berlin, 1988).
[42] J. M. Bennett, J. L. Stanford and E. J. Ashley, J. Opt. Soc. Am. 60, 224–231 (1970).
[43] A. J. Varkey and A. F. Fort, Sol. Energ. Mat. Sol. Cells 29, 253–259 (1993).
[44] F.-M. Becker, G. Boortz, V. Dietrich, L. Engelmann, C. Ernst et al., in 'Formeln und Tabellen', Ed. By F.-M. Becker, G. Boortz, V. Dietrich, L. Engelmann, C. Ernst et al. (Duden Paetec Schulbuchverlag, Berlin, 2005) p. 17.
[45] U. Kreibig, J. Phys. F Met. Phys. 4, 999 (1974).
[46] H. Ehrenreich and H. R. Philipp, Phys. Rev. 128, 1622–1629 (1962).
[47] V. Linss, O. Stenzel and D. R. T. Zahn, J. Raman Spectrosc. 30(7), 531–536 (1999).
[48] J. Gäbler, in 'Entwicklung und Charakterisierung eines Messeinsatzes zur simultanen Erfassung des Transmissions- und Reflexionsvermögens im visuellen Spektralbereich für Hochvakuum-Bedampfungsprozesse', Bachelor thesis (Erst-Abbe-Fachhochschule/Fraunhofer IOF, Jena, 2013).
[49] R. M. A. Azzam and A. Alsamman, Appl. Optics 47, 3211–3215 (2008).
[50] A. V. Tikhonravov, M. K. Trubetskov, A. A. Tikhonravov and A. Duparre, Appl. Optics 42, 5140–5148 (2003).
[51] O. Stenzel, in 'The physics of thin film optical spectra. An introduction', Ed. By G. Ertl, H. Lüth and D. L. Mills (Springer-Verlag, Berlin, 2005) pp. 45–60.
[52] O. Stenzel and A. Macleod, Adv. Opt. Technol. 1, 463–481 (2012).